Vietnam Journal of Science and Technology ***60*** *(2) (2022) 245-256*

doi:10.15625/2525-2518/16212

STRUCTURAL, ELECTRICAL AND FERROELECTRIC PROPERTIES OF $NiTiO_3$ NANOPARTICLES SYNTHESIZED BY CITRATE-GEL METHOD

Chu Duc Viet[1], Nguyen Tuyet Nga[1], Do Duc Tho[1], Tran Vu Diem Ngoc[2], Nguyen Van Dung[1], Luong Huu Bac[1, *]

[1]*School of Engineering Physics, Hanoi University of Science and Technology, 1 Dai Co Viet Road, Ha Noi, Viet Nam*

[2]*School of Materials Science and Engineering, Hanoi University of Science and Technology, 1 Dai Co Viet Road, Ha Noi, Viet Nam*

[*]Emails: *bac.luonghuu@hust.edu.vn*

Received: 27 June 2021; Accepted for publication: 22 November 2021

Abstract. In this work, we carried out a study on $NiTiO_3$ nanomaterial synthesized via citrate-gel method. The structural characteristics were determined by basic X-ray diffraction analysis. SEM analysis showed the surface morphology of the sample. The impedance spectra analysis was used to elucidate the dependence of complex impedance values on temperature and frequency. The correlation between DC conductivity and the inverse temperature values was presented and it complied with semiconductor behavior of Arrhenius type. The real dielectric constant (ε'), the dielectric loss (tan δ) and the AC conductivity values were reported as a function of frequency ranging from 1 kHz to 10 MHz at different temperatures (25 ^oC - 500 ^oC). The dielectric constant decreased quickly with increasing of frequency in range from 1 kHz to 100 kHz and almost kept constant when the frequency was in range from 100 kHz to 10 MHz. Loss tangent of $NiTiO_3$ material had value of 0.02 at 400 ^oC and frequency of 1 MHz. It increased with decreasing of frequency and reached to 2.9 at frequency of 1 kHz. Conductivity was found to obey Jonscher's power law of conductivity. The room temperature polarization-electric field loops were examined. Ferroelectricity was observed in $NiTiO_3$ sample at room temperature and maximum polarization increased with increasing polarization electric field.

Keywords: citrate gel method, impedance, dielectric properties, electrical conductivity.

Classification numbers: 2.2.2, 2.9.2, 2.10.3.

1. INTRODUCTION

$MTiO_3$ (M = Ni, Fe, Mn) compounds are considered as potential candidates for application in many fields because they can be adapted in visible-light photocatalysis [1], solid oxide fuel cells [2], gas or glucose sensor [3, 4], spin electronic devices with magnetoelectric effect [5], paint pigment [6], and anode materials for lithium-ion batteries [7] due to its multifunctional ability. Among them, $NiTiO_3$ has an ilmenite type, with both Ni and Ti having octahedral

coordination and Ni^{2+} and Ti^{4+} alone occupying the alternating cation layers [8]. $NiTiO_3$ is an *n*-type semiconductor with a low bandgap of around 2.18 eV. Due to its low bandgap value, this material is applied for visible-light-driven photocatalysis to harvest visible light. Recently, $NiTiO_3$ materials have attracted considerable attention because of their high photocatalytic activity under UV irradiation and remarkably under visible light [9 - 11]. $NiTiO_3$ ilmenite materials have been known to show interesting magnetic and electric properties [12]. According to previous studies on $NiTiO_3$, these materials have semiconducting and antiferromagnetic properties [13]. The magnetic investigation showed the antiferromagnetic transition at 14.9 K and the magnetic moment was 4.7 μ_B [14]. It has also gained attention in the field of semiconductor devices because of its high dielectric constant. Again, $NiTiO_3$ is stable and can be applied in high-temperature environments. Recently, $NiTiO_3$ has received much attention owing to high solar reflectance in near-infrared radiation, and it has been used as cool pigments for building coatings [15].

$NiTiO_3$ materials have been synthesized by various methods such as solid-state [12], sol-gel [17], molten salt [14], polymer [18] methods. In this paper, the citrate-gel method was used because it has many advantages such as easy to process and control the structure, extended composition ranges, good homogeneity, and low energy consumption [19]. The citrate-gel method is a reliable process to synthesize inorganic nanomaterials including binary, ternary, and quaternary metal oxides with a homogeneous distribution of components on the atomic scale. This process was carried out at lower temperature than that of the solid-state route therefore it used less energy. Moreover, it requires simple equipment and easy operation, as well as allows to prepare materials with high purity and high yields of ultrafine powders. The key advantage of this method is to keep the homogeneity of the starting material from solution to gel. Our group has successfully synthesized $NiTiO_3$ nanomaterials by the citrate method [20]. In this work, we presented the analysis of electrical properties of ilmenite $NiTiO_3$ which was synthesized by a simple low-cost citrate gel method

2. MATERIALS AND METHODS

Nickel (II) titanate ($NiTiO_3$) nanoparticles were synthesized using the citrate-gel method. In a typical process, acid citric was dissolved in distilled water at room temperature. Then titanium isopropoxide ($C_{12}H_{28}O_4Ti$) was added to the solution, which was continuously stirred at 70 ^oC until it becomes transparent. Nickel (II) nitrate ($Ni(NO_3)_2$) was added to the above solution, which was then continuously stirred for 4 h to dehydrate until it turned into a gel form. The gel was dried at 120 ^oC for 1 day to obtain xerogel, which was fired at 400 ^oC for 2 h and then calcined in an oven at 700 ^oC for 3 h. The obtained powders were ground in an agate mortar for analysis. XRD measurement was implemented by a X-ray diffractometer PAN alytical X'pert Pro powder with Cu Kα radiation. The micrograph of the synthesized powder and the sintered pellets was recorded by a field emission scanning electron microscope (FESEM).

For electrical characterization, the obtained powder was mixed with a small amount of polyvinyl alcohol to constitute a homogeneous mixture. The resulting mixture was pressed into pellets with a diameter of 10 mm and a thickness of 1.5 mm using a uniaxial hydraulic press at a pressure of 10^6 N/m^2. The pellets were sintered at 1200 ^oC for 5 h in the air atmosphere. A thin layer of silver was coated on both sides of the sintered samples to make the surface parallel and then heated at 500 ^oC for 30 min.

Impedance spectroscopy of the $NiTiO_3$ samples was carried out using an HP - 4192A impedance analyzer over a frequency range of 1 kHz to 10 MHz and in the temperature range

from room temperature up to 500 ^oC. A *P–E* hysteresis loop tracer (Radiant Technologies, Inc.) was used to trace the electrical hysteresis loops.

3. RESULTS AND DISCUSSION

3.1. Structural analysis

The phase purity of synthesized materials was analyzed by the X-ray diffraction method. Figure 1 shows the X-ray diffraction pattern of the $NiTiO_3$ sample. All diffraction peaks observed at 2θ = 24.03°, 32.99°, 35.55°, 40.76°, 49.34°, 53.90°, 57.35°, 62.35°, and 63.97° are matched with the rhombohedral crystal structure (JCPDS 83-0198). No impurity peaks were found in the XRD pattern which confirms that the obtained material was homogeneous and was in a single-phase. The lattice parameters were evaluated using the UNITCELL-97 program and were found to be a = b = 5.031 Å and c = 13.798 Å. The Scherrer crystallite sizes were calculated using all the diffraction peaks appearing in the patterns, according to Scherrer formula $L = k\lambda/\beta\cos\theta$, where λ is the wavelength of the X-ray radiation (Cu K_α = 0.15406 nm), k is the constant, β is the line width at half maximum height, and θ is the diffracting angle. The crystalline grain size calculated by the Scherrer formula was 54 nm.

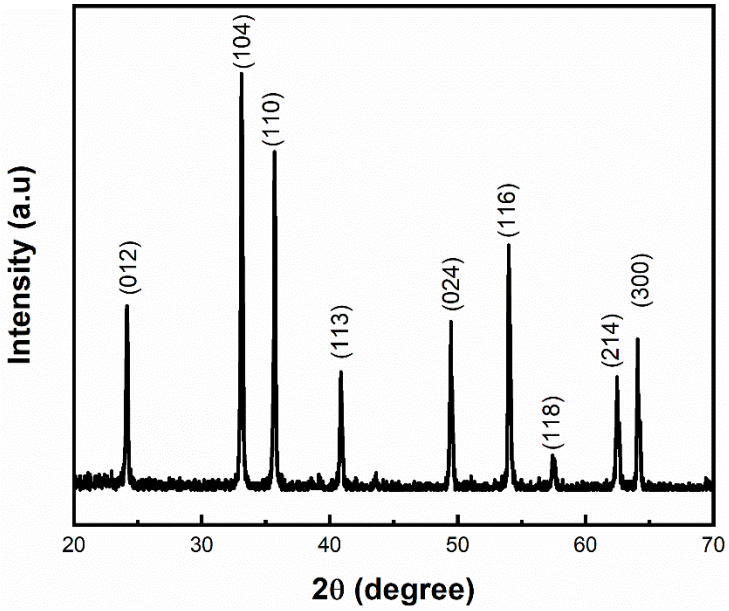

Figure 1. X-ray diffraction pattern of $NiTiO_3$ synthesized by the citrate-gel method.

Figure 2a shows an SEM image of the $NiTiO_3$ powder sample after being calcined at 700 ^oC for 3 h. It can be seen that the grains are almost spherical in shape. The average size of grains is 134.8 ± 38.7 nm. Figure 2b shows an SEM image of the pellet surface sintered at 1200 ^oC for 5 h. It is clear that the grain growth of nanopowders caused the grain much bigger. It changed from the nano-size in the as-synthesized powder to microsize in the sintered sample. Due to high temperature sintering, the powders were sintered, creating a dense sample. The average grain size was 3.7 ± 1.6 μm for the sintered sample.

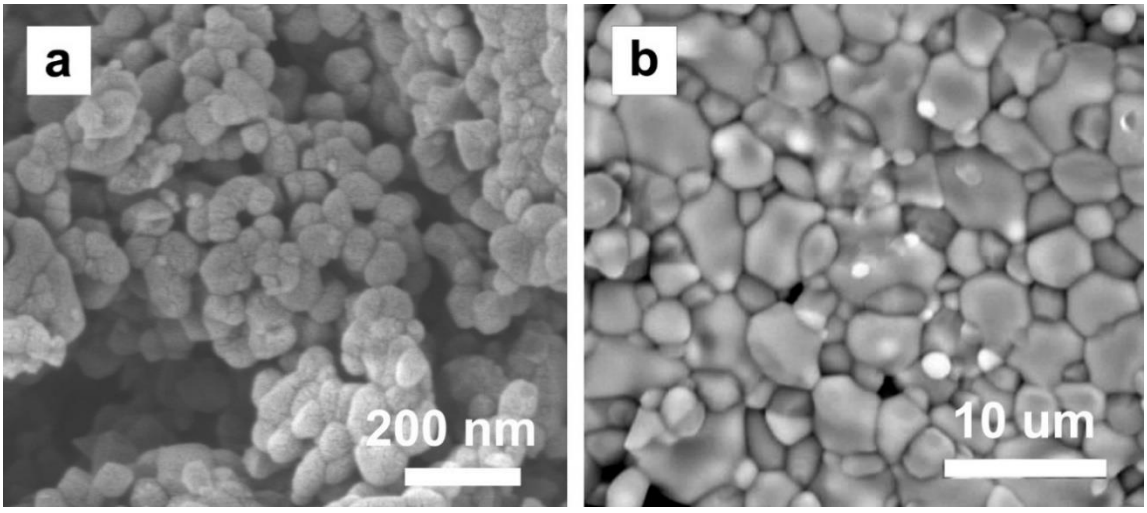

Figure 2. SEM images of a) $NiTiO_3$ powder calcined at 700 ^oC for 3 h and b) the pellet surface sintered at 1200 ^oC for 5 h.

3.2. Electrical analysis

3.2.1. Impedance spectrum

The impedance spectral analysis provides comprehension of various elements contributing to the electrical properties of the material. The Cole-Cole plots are plotted over a wide frequency range at different temperatures. They are expressed via the real parts Z' and the imaginary parts Z" of the impedance.

Figure 3 shows the Cole-Cole plots of impedance spectra for $NiTiO_3$ sample in a temperature range of 400 ^oC - 500 ^oC. As it is clearly observed from the figure, a single semicircle occurring in the high-frequency region is associated with the bulk conduction of the material. A decreasing trend is seen at the impedance values when the temperature increases from 400 ^oC to 500 ^oC. The centers of the semicircles lie below the real axis referred to as non-Debye relaxation. Generally, the cases of non-Debye type are explained by the parameter α ($0 < \alpha < 1$). For $\alpha = 1$, the center of semicircles lies on the real axis. In the case of $NiTiO_3$ ceramic, the α is 0.952 for the impedance spectrum of the sample measured at 400 ^oC. The behavior of the Cole-Cole plots can be attributed to the contribution of a parallel circuit of capacitance C_b and resistance R_b. The inset of Figure 3 depicts the equivalent RC circuit of the bulk conductance of $NiTiO_3$. Each semicircle corresponding to each temperature has its relaxation frequency which is expressed by the following formula [21]:

$$\tau = \frac{1}{\omega} = R_b.C_b \quad (1)$$

where $\omega = 2\pi f_{max}$, f_{max} is the relaxation frequency, and τ is relaxation time. No semicircle can be seen in the low-frequency region that indicates that the conduction contributed by grain boundary does not appear in the Cole-Cole plots and only conduction contributed by bulk appears. The values of bulk resistance R_b are determined by the interception of the semicircles with the x-axis. The diameter of the semicircle is obtained by fitting to an equivalent circuit model using the software Ivium.

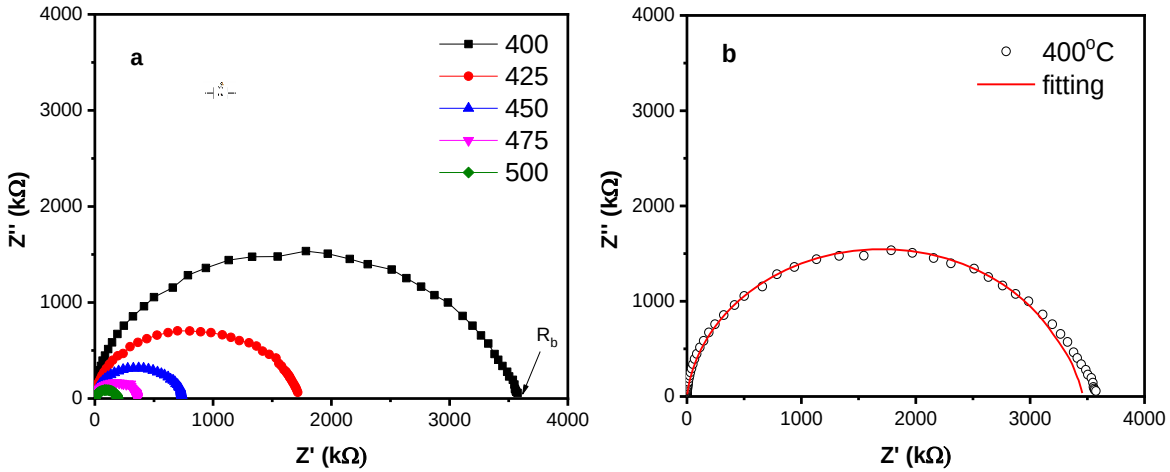

Figure 3. a) Impedance spectra of the $NiTiO_3$ sample at different temperatures and b) fitting curve of the impedance spectrum of the $NiTiO_3$ sample measure at 400 ^oC.

The DC-conductivity is calculated from the collected R_b values using the following formula [21]:

$$\sigma_{dc} = \frac{t}{SR_b} \tag{2}$$

where t is thickness, S is the cross-sectional area of the pelletized $NiTiO_3$ sample (in cm) and σ_{dc} is the DC-conductivity ($S.cm^{-1}$). The relation $\omega.R_b.C_b = 1$ or $2\pi f_{max}.R_b.C_b = 1$ is used to determine the bulk capacitance values. Thus, the relaxation time τ can be assessed from the values of R_b and C_b. The calculated values are listed in Table.1. The value of bulk capacitance is in order of picofarads (pF). The relaxation time decreased with increasing temperature which indicated that the diffusion of the carriers was a thermally activated phenomenon. The higher relaxation time implied a slower relaxation process. Moreover, the decrement of resistance and increasing of DC conductivity when temperature increased revealed the semiconducting nature of material containing the negative temperature coefficient behavior. The value of DC conductivity was 1.37×10^{-6} $S.cm^{-1}$ at 500 ^oC.

3.2.2. Conductance spectral analysis

Electrical conduction in the dielectric material is a thermal activation process. The conductance is the ordered motion of weakly bound charged particles under the electric field. It depends on the nature of the charge carriers. The temperature-dependence of the DC conductivity of ceramics can be expressed through the following Arrhenius equation [22].

$$\sigma_{dc} = \sigma_o \exp\left(-\frac{E_a}{k_B T}\right) \tag{3}$$

where σ_{dc} is the conductivity at temperature T, σ_0 is called the pre-exponential factor, k_B is Boltzmann's constant and E_a is the activation energy. The relation between DC-conductivity values $\ln(\sigma_{dc})$ and the inverse of temperature (1000/T) is represented in Figure 4. The plot shows the linearity of the values as the result of thermally activated behavior. It is evident that (σ_{dc}) values increase with the increase of temperature indicating that the conduction is a thermally activated process. This phenomenon explained the hopping of charge carriers which was more mobility at higher temperatures. The activation energy for the sample was estimated from the

linear fitting of the curve in Figure 4. The activation energy for the sample was 1.2 eV for the high-temperature region and 0.05 eV for the low-temperature region. These values prove that a small amount of energy is sufficient to activate the charge carriers for electrical conduction. The activation energy for the $NiTiO_3$ sample is higher than that for the $NiTiO_3$ sample synthesized by the solid-state method at high-temperature region. It may be related to the crystalline size of the materials. $NiTiO_3$ material synthesized by the citrate gel method had a smaller crystalline size than that of the one synthesized by the solid-state method which leads to an increase in the effective potential barrier height for electrical conduction [12]. The DC conductivity value of $NiTiO_3$ material was lower compared with those of $NiTiO_3$ material synthesized by the solid-state method.

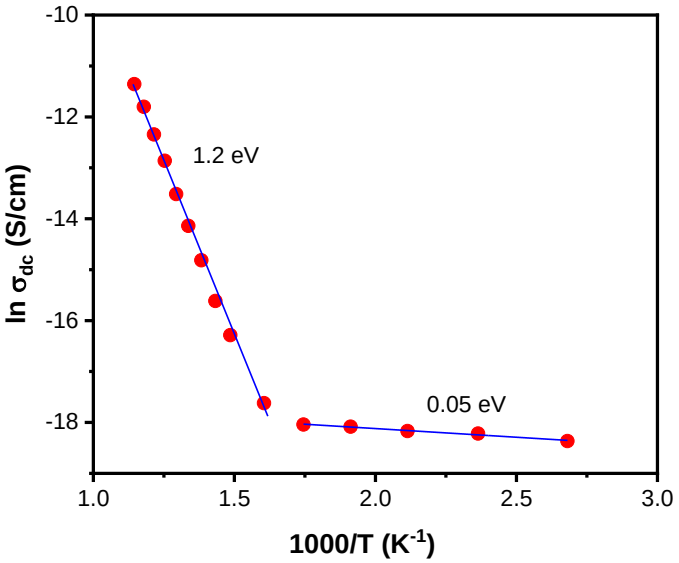

Figure 4. Arrhenius plot of DC conductivity for the $NiTiO_3$ sample.

Table 1. Conductance parameters at different temperatures of $NiTiO_3$.

Temperature (^oC)	R_b (MΩ)	C_b (pF)	τ (μs)	σ_{dc} ($S.cm^{-1}$)
400	3.40	1.87	6.36	$7.63x10^{-8}$
425	1.60	3.42	5.47	$1.63x10^{-7}$
450	0.71	4.22	3.00	$3.66x10^{-7}$
475	0.36	5.55	1.98	$7.26x10^{-7}$
500	0.19	7.12	1.35	$1.37x10^{-6}$

Figure 5 shows the dependence of ac-conductivity values ($\sigma_{(\omega)}$) on the frequency at a temperature range of 400 ^oC - 500 ^oC. The frequency dependence of the conductivity of the $NiTiO_3$ ceramic exhibits both low- and high-frequency dispersion phenomena. The dependence of conductivity on the frequency obeys Jonscher's power law [23] as presented below:

$$\sigma(\omega) = \sigma_{dc} + A\omega^n \quad (4)$$

where n is the frequency exponent that infers the degree of interactions between the mobile ions and the lattices, σ_{dc} and A are thermally activated quantities. The nonlinear curve fitting was

done and shown in Figure 6 which indicated that the conductivity of $NiTiO_3$ ceramics was based on Jonscher's power law. The value of n was about 1.05. According to Funke [24], $n > 1$ means that the motion involves localized hopping without the species leaving the neighborhood. The AC-conductivity curves in the lower frequency region (1 kHz - 100 kHz) remain constant because of the low and steady conductance. The conductance increased when the frequency grew up to the range from 100 kHz to 10 MHz, which demonstrates the dominant contribution of grains to the conduction compared to the contribution of grain boundaries.

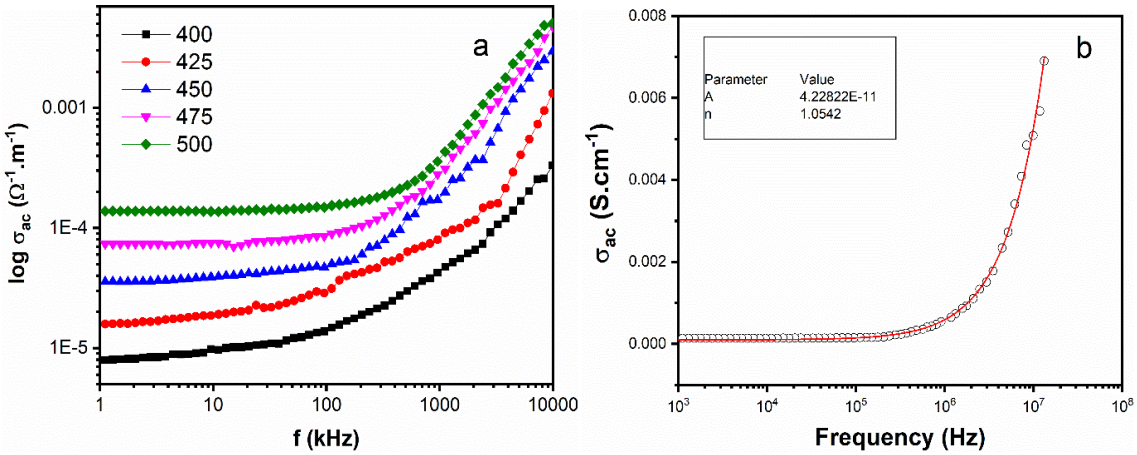

Figure 1. a) Frequency dependence of AC-conductivity of $NiTiO_3$ and b) Non-linear curve fitting of conductance spectra at 500 ^oC.

3.2.3. Dielectric analysis

The relative dielectric constant ε_r^* is separated into two parts, the real dielectric ε' and the dielectric loss factor ε'', which can be expressed via the following relation as a function of angular frequency ω [25]:

$$\varepsilon_r^*(\omega) = \varepsilon_r'(\omega) + j\varepsilon_r''(\omega) \tag{5}$$

The dielectric loss factor is a measurement of the energy absorbed in the medium as an electromagnetic wave passes through that medium. The loss of energy involved in heating a dielectric material in an assorted electric domain is called dielectric loss.

The dielectric constant (ε') and dielectric loss ($\tan\delta$) were calculated from complex impedance data using the following expressions [26]:

$$\varepsilon'(\omega) = \frac{t}{2\pi f \varepsilon_o S}\frac{z''}{|Z|^2} \tag{6}$$

$$\varepsilon''(\omega) = \frac{t}{2\pi f \varepsilon_o S}\frac{z'}{|Z|^2} \tag{7}$$

$$\tan\delta = \frac{\varepsilon''}{\varepsilon'} \tag{8}$$

where Z', Z'' represent the real and imaginary parts of the impedance, respectively and ε_o is the absolute dielectric permittivity of vacuum, S is the cross-sectional area of the pelletized $NiTiO_3$ sample, and |Z| represents the impedance modulus.

In this research, the frequency dependence of the real dielectric ε′ and the dielectric loss tangent tan δ in an applied AC field was observed over a temperature range of 400 ^{o}C – 500 ^{o}C at various frequency regions (1 kHz - 10 MHz). Figure 6 shows the variation of the real dielectric constant and loss tangent according to the frequency. In the lower frequency range from 1 kHz to 100 kHz, the real dielectric values decline quickly with increasing frequency, then it is clear that these values attain the saturation limit when the frequency is over 100 kHz. A similar trend can be seen in Figure 6b when the loss tangent values decrease as the frequency increases gradually.

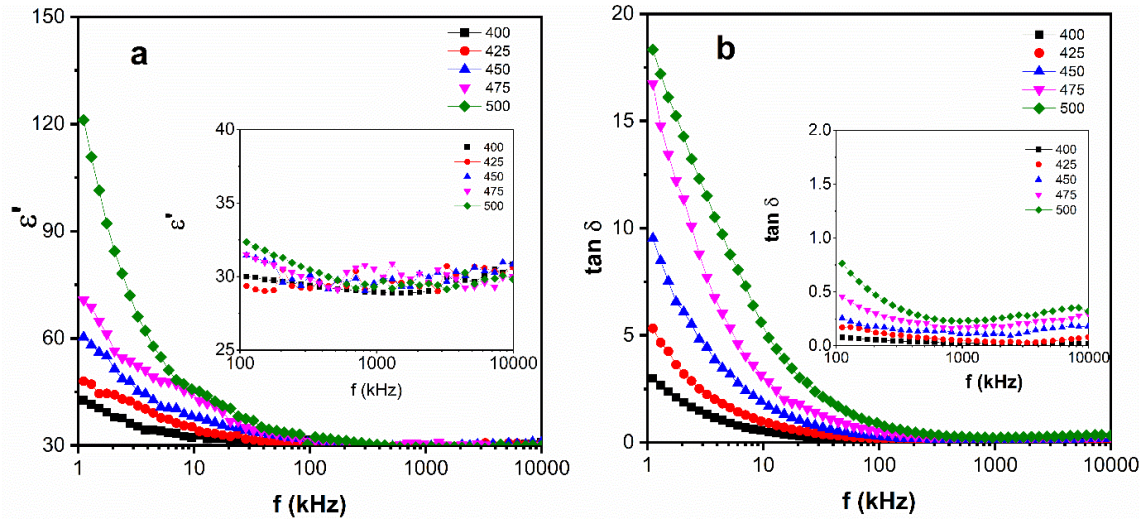

Figure 6. Variation of (a) real dieletric constant ε′ and (b) loss tangent tan δ with frequency at different temperatures of $NiTiO_3$ (the inset shows the enlarged frequency region from 100 kHz to 10 MHz).

The multiple types of polarization (ionic, electronic, dipolar, interfacial, or space charge) are considered as the reason of the variation of real dielectric constant and loss tangent with frequency at different temperatures. The dipolar polarization and space-charge polarization are believed that they have the most significance at low frequencies [27]. Therefore, the real dielectric constant is greater in the low-frequency region. In contrast, the contribution of space-charge and other polarization is trivial at higher frequencies and the electronic polarization is the only element having a contribution to the dielectric constant. Thus, the real dielectric constant is small at higher frequencies. The same decreasing trend can be seen in the loss tangent. This indicates a common behavior of compounds with mobile carriers [28].

Figure 7 depicts the variation of real dielectric constant ε′ as a function of temperature at some selected frequencies from 100 kHz to 10 MHz. The value of the real dielectric constant remains almost stable at the high-frequency region from 100 kHz to 10 MHz which shows the temperature independence of the real dielectric constant. In the lower frequency region from 1 kHz to 100 kHz, the real dielectric constant increases gradually with increasing temperature. This phenomenon occurs due to the presence of space-charge polarization in the powder sample. Space-charge or interfacial polarization is attributed to the accumulation of charge carriers in the space among grains. This is very common in dielectric materials under an applied external field and when two electrodes are connected to a dielectric material as well. Grain or particle size increases with temperature. Increased grain size hinders the flow of charge carriers and hence augment the dielectric constant values [29].

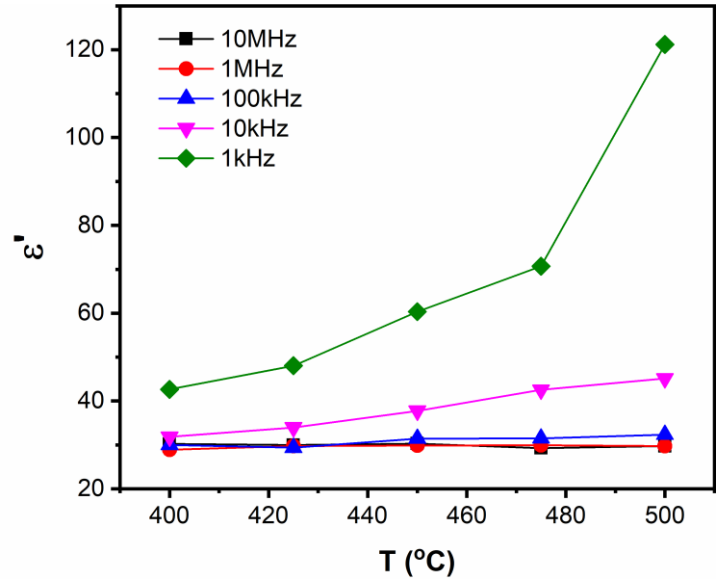

Figure 7. Variation of real dielectric constant ε' with temperature at several frequencies of $NiTiO_3$.

3.3. Ferroelectric properties analysis

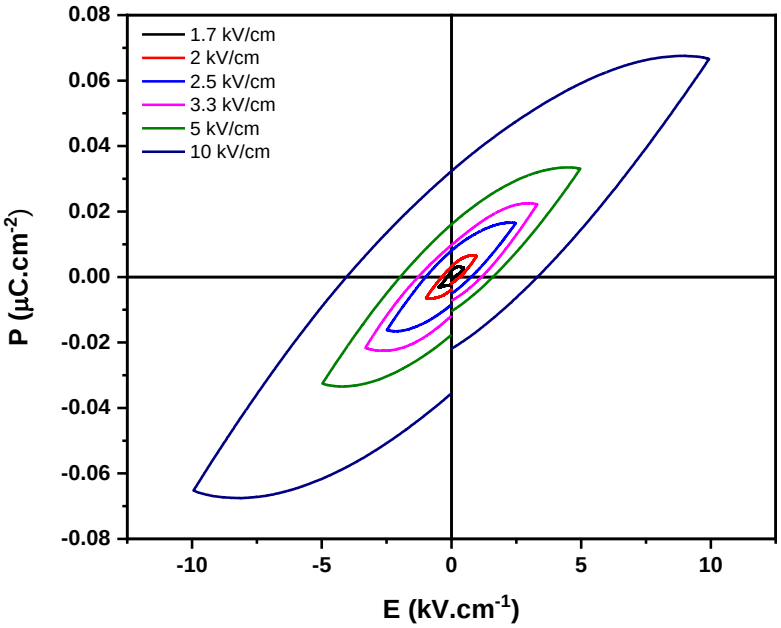

Figure 8. P-E hysteresis loops measured on sintered pellets of $NiTiO_3$ at different polarizing electric fields.

Figure 8 displays the hysteresis loops (P–E) of $NiTiO_3$ at various applied electric fields. The nature of hysteresis loops indicates the existence of ferroelectricity and dynamic polarisability in the material. The nature of the *P–E* hysteresis loop of $NiTiO_3$ confirms its ferroelectric properties. Figure 8 shows the well-developed, symmetric, and saturated ferroelectric hysteresis loops for the $NiTiO_3$sample. The saturation polarization (P_s) of $NiTiO_3$ at

room temperature is found to be 0.07 μC/cm^2 at an electric field of 10 kV/cm and the coercive field is 3.37 kV/cm. This *P–E* hysteresis loop indicated the different behavior with $NiTiO_3$ sample fabricated by the solid-state method.

According to a study by Truptimatyee Acharya *et al*. [12], the $NiTiO_3$ fabricated by solid-state method and its ferroelectric behaviour show that it has a much smaller coercive field and much larger saturation polarization in comparison with the values of $NiTiO_3$ synthesized by the citrate gel method. The value of saturation polarization and coercive field of $NiTiO_3$ fabricated by the solid-state method were 3.932 μC/cm^2 and 0.85 kV/cm, respectively. The difference in the coercive field and saturation polarization of $NiTiO_3$ ceramic may be related to the phase, microstructure, and microstrain of the fabricated $NiTiO_3$ pellets. In general, the particle size of the sample fabricated by the solid-state method is much larger than that synthesized by the wet chemical method. However, it needs more evidence and data to correlate the synthesis method and microstructure influencing the ferroelectric properties of $NiTiO_3$.This section describes clearly the observations made and their concise interpretation. Results should be presented in tables and/or figures whenever possible, and should be clearly explained in the text. Be aware of inserting them close to the point of their discussion, and not dividing each of them onto different pages. One paragraph must not contain only one sentence.

4. CONCLUSIONS

In conclusion, $NiTiO_3$ nanoparticles were successfully synthesized via the citrate-gel method. XRD analysis confirmed the rhombohedral crystal structure and R3 space group of the sample. SEM images showed the morphology and grain growth of $NiTiO_3$ in powder and pellet forms. Impedance spectroscopy showed the semicircles with the center of each semicircle below the x-axis that indicated non-Debye relaxation. Conductance analysis confirmed the semiconducting features of $NiTiO_3$. The DC conductivity values increase with increasing temperature and the frequency dependence of ac-conductivity was shown as well. The dielectric properties of $NiTiO_3$ were also investigated over a wide range of frequency (1 kHz - 10 MHz) at different temperatures. The nature of the hysteresis loop shows that the material has ferroelectric characteristics at room temperature. This study shows that $NiTiO_3$ exhibits many potential behaviors that can be useful for multifunctional devices.

Acknowledgements. This research is funded by Vietnam Ministry of Education and Training (MOET) under Grant number B2021-BKA-02.

CRediT authorship contribution statement. Chu Duc Viet: Materials synthesis and measurement impedance spectroscopy. Nguyen Tuyet Nga: Methodology, Investigation. Do Duc Tho: Structurral analysis. Tran Vu Diem Ngoc: electrical analysis. Nguyen Van Dung: Electrical analysis. Luong Huu Bac: Writing, Formal analysis, Supervision.

Declaration of competing interest. The authors declare that they have no known competing financial interests or personal relationships that could have appeared to influence the work reported in this paper.

REFERENCES

1. Jing P., Lan W., Su Q., Yu M., Xie E. - Visible-Light Photocatalytic Activity of Novel $NiTiO_3$ Nanowires with Rosary-Like Shape, Science of Advanced Materials **6** (2014) 434-440.

2. Wang Z., Wang Z., Yang W., Peng R., Lu Y. - Carbon-tolerant solid oxide fuel cells using $NiTiO_3$ as an anode internal reforming layer, Journal of Power Sources **255** (2014) 404-409.
3. Della Gaspera E., Pujatti M., Guglielmi M., Post M. L., Martucci A. - Structural evolution and hydrogen sulfide sensing properties of $NiTiO_3$–TiO_2 sol–gel thin films containing Au nanoparticles, Materials Science and Engineering: B. **176** (2011) 716-722.
4. Huo K., Li Y., Chen R., Gao B., Peng C., Zhang W., Hu L., Zhang X., Chu P. K. - Recyclable non-enzymatic glucose sensor based on Ni/$NiTiO_3$/TiO_2 nanotube arrays, Chem. Plus Chem. **80** (2015) 576-582.
5. Jaye K., Moureen C., Harada J. K., Balhorn L., Hazi J., Kemei M. C., Seshadri R. - Magnetodielectric coupling in the ilmenites $MTiO_3$ (M = Co , Ni), Phys. Rev. B. **93** (2016) 104404.
6. Moghtada A., Shahrouzianfar A., Ashiri R. - Dyes and Pigments Facile synthesis of $NiTiO_3$ yellow nano-pigments with enhanced solar radiation reflection efficiency by an innovative one-step method at low temperature, Dyes and Pigments **139** (2017) 388-396.
7. Lu C., Naresh N., Kumar P. S., Som S. - Microwave-assisted solvothermal synthesis and electrochemical characterizations of ternary perovskite $NiTiO_3$ anode materials for lithium-ion batteries, Ceramics International, 2019.
8. Lerch M., Boysen H., Neder R., Frey F., Laqua W. - Neutron scattering investigation of the high temperature phase transition in $NiTiO_3$, Journal of Physics and Chemistry of Solids **53** (1992) 1153-1156.
9. Shu X., He J., Chen D. - Visible-Light-Induced Photocatalyst Based on Nickel Titanate Nanoparticles **2** (2008) 4750-4753.
10. Sadjadi M. S., Mozaffari M., Enhessari M., Zare K. - Effects of $NiTiO_3$ nanoparticles supported by mesoporous MCM-41 on photoreduction of methylene blue under UV and visible light irradiation, Superlattices and Microstructures **47** (2010) 685-694.
11. El-Maghrabi H. H., Nada A. A., Diab K. R., Youssef A. M., Hamdy A., Roualdes S., Abd El-Wahab S. - Facile fabrication of $NiTiO_3$/graphene nanocomposites for photocatalytic hydrogen generation, Journal of Photochemistry and Photobiology A: Chemistry **365** (2018) 86-93.
12. Acharya T., Choudhary R. N. P. - Structural, Ferroelectric, and Electrical Properties of $NiTiO_3$ Ceramic, Journal of Electronic Materials **44** (2014) 271-280.
13. Van Uitert L. G., Sherwood R. C., Williams H. J., Rubin J. J., Bonner W. A. - Magnetic properties of a number of divalent transition metal tungstates, molybdates and titanates, Journal of Physics and Chemistry of Solids **25** (1964) 1447-1451.
14. Yuvaraj S., Nithya V. D., Fathima K. S., Sanjeeviraja C., Selvan G. K., Arumugam S., Selvan R. K. - Investigations on the temperature dependent electrical and magnetic properties of $NiTiO_3$ by molten salt synthesis, Materials Research Bulletin **48** (2013) 1110-1116.
15. He X., Wang F., Liu H., Li J., Niu L. - Synthesis and coloration of highly dispersed $NiTiO_3$@ TiO_2 yellow pigments with core-shell structure, Journal of the European Ceramic Society **37** (2017) 2965-2972.
16. Acharya R. N. P., T. and Choudhary - Structural, Ferroelectric, and Electrical Properties of $NiTiO_3$ Ceramic, Journal of Electronic Materials **44** (2015) 271-280.

17. Ruiz-Preciado M. A., Kassiba A., Gibaud A., Morales-Acevedo A. - Comparison of nickel titanate ($NiTiO_3$) powders synthesized by sol-gel and solid state reaction, Materials Science in Semiconductor Processing **37** (2015) 171-178.
18. Lopes K. P., Cavalcante L. S., Sim A. Z., Varela J. A., Longo E., Leite E. R. - $NiTiO_3$ powders obtained by polymeric precursor method: Synthesis and characterization, Journal of Alloys and Compounds **468** (2009) 327-332.
19. Danks A. E., Hall S. R., Schnepp Z. - The evolution of 'sol–gel' chemistry as a technique for materials synthesis, Materials Horizons **3** (2016) 91-112.
20. Van Thang P., D. D. Dung, Bac L. H., Hung P. P., Ngoc T. V. Di. - Structural, Optical, Ferroelectric and Magnetic Properties of $NiTiO_3$ Ceramic Synthesized by Citrate Gel Method, International Journal of Nanoscience **20** (2021) 1-7.
21. Rout S. K., Hussian A., Lee J. S., Kim I. W., Woo S. I. - Impedance spectroscopy and morphology of $SrBi_4Ti_4O_{15}$ ceramics prepared by soft chemical method, Journal of Alloys and Compounds **477** (2009) 706-711.
22. Pu Y., Dong Z., Zhang P., Wu Y., Zhao J., Luo Y. - Dielectric, complex impedance and electrical conductivity studies of the multiferroic $Sr_2FeSi_2O_7$-crystallized glass-ceramics, Journal of Alloys and Compounds **672** (2016) 64-71.
23. Jonscher A. K. - The 'universal'dielectric response, Nature **267** (1977) 673-679.
24. Funke K. - Jump relaxation in solid electrolytes, Progress in Solid State Chemistry **22** (1993) 111-195.
25. Tian F., Ohki Y. - Electric modulus powerful tool for analyzing dielectric behavior, IEEE Transactions on Dielectrics and Electrical Insulation **21** (2014) 929-931.
26. Lanfredi S., Gênova D. H. M., Brito I. A. O., Lima A. R. F., Nobre M. A. L. - Structural characterization and Curie temperature determination of a sodium strontium niobate ferroelectric nanostructured powder, Journal of Solid State Chemistry **184** (2011) 990-1000.
27. West L. L., Hench J. K. - Principles of Electronic Ceramics, Wiley-Interscience; 1st edition, 1990.
28. Anderson J. C. - Dielectrics, London: Chapman and Hall, 1964.
29. Bamzai K. K., Gupta V., Kotru P. N., Wanklyn B. M. - Dielectric and A.C conductivity behaviour of flux grown Nickel titanate ($NiTiO_3$) crystal, Ferroelectrics **413** (2011) 328-341.